J Seismol (2008) 12:107–123
DOI 10.1007/s10950-007-9074-y

ORIGINAL ARTICLE

Recent seismicity in Northeast India and its adjoining region

Kiran Kumar Singh Thingbaijam · Sankar Kumar Nath · Abhimanyu Yadav · Abhishek Raj · M. Yanger Walling · William Kumar Mohanty

Received: 11 May 2007 / Accepted: 12 November 2007 / Published online: 13 December 2007

Abstract Recent seismicity in the northeast India and its adjoining region exhibits different earthquake mechanisms – predominantly thrust faulting on the eastern boundary, normal faulting in the upper Himalaya, and strike slip in the remaining areas. A homogenized catalogue in moment magnitude, M_W, covering a period from 1906 to 2006 is derived from International Seismological Center (ISC) catalogue, and Global Centroid Moment Tensor (GCMT) database. Owing to significant and stable earthquake recordings as seen from 1964 onwards, the seismicity in the region is analyzed for the period with spatial distribution of magnitude of completeness m_t, b value, a value, and correlation fractal dimension D_C. The estimated value of m_t is found to vary between 4.0 and 4.8. The a value is seen to vary from 4.47 to 8.59 while b value ranges from 0.61 to 1.36. Thrust zones are seen to exhibit predominantly lower b value distribution while strike-slip and normal faulting regimes are associated with moderate to higher b value distribution. D_C is found to vary from 0.70 to 1.66. Although the correlation between spatial distribution of b value and D_C is seen predominantly negative, positive correlations can also be observed in some parts of this territory. A major observation is the strikingly negative correlation with low b value in the eastern boundary thrust region implying a possible case of extending asperity. Incidentally, application of box counting method on fault segments of the study region indicates comparatively higher fractal dimension, D, suggesting an inclination towards a planar geometrical coverage in the 2D spatial extent. Finally, four broad seismic source zones are demarcated based on the estimated spatial seismicity patterns in collaboration with the underlying active fault networks. The present work appraises the seismicity scenario in fulfillment of a basic groundwork for seismic hazard assessment in this earthquake province of the country.

Keywords b value · a value · Correlation fractal dimension · Northeast India · Seismicity

K. K. S. Thingbaijam · S. K. Nath (✉) · A. Yadav · A. Raj · M. Y. Walling · W. K. Mohanty
Department of Geology and Geophysics,
Indian Institute of Technology,
Kharagpur, India
e-mail: nath@gg.iitkgp.ernet.in

1 Introduction

The northeast Indian region has been placed in zone V, the highest level of seismic hazard potential, according to the seismic zonation map of India (BIS 2002). As such there have been incidents of two great earthquakes – 1897 Shillong Earthquake, and 1950 Assam Earthquake in the region. The Global Seismic Hazard Assessment Programme (GSHAP) also classifies the region in the zone of high seismic risk with

peak ground acceleration rising to the tune of 0.35–0.4g (Bhatia et al. 1999). Moreover, rapid urbanization in the region have provided a higher level of man-made constructions deviating from the typical Assam-type houses to multistoried structures and a significant population outburst as compared to the time of occurrence of great earthquakes, thereby implicating increased vulnerability to earthquake disasters.

In the present study, contemporary perspectives on seismicity and seismotectonic setting of the study region are examined. Region specific earthquake magnitude scaling relations correlating different magnitude scales are achieved to develop a homogenous catalogue in moment magnitude, M_W, for the region. The different aspects of spatial seismicity are quantified through spatial distribution of seismicity parameters – magnitude of completeness or threshold magnitude m_t, a and b values, and correlation fractal dimension D_C of the epicenters. Thereafter, the seismotectonic disparities in the region are correlated with the spatial variation of seismicity parameters. The predominant fault segments in the region are also examined by box counting fractal dimension, D. The results of the spatial seismicity analysis in conjunction with the organization of active fault networks are employed to classify broad seismic source zones.

2 Regional tectonic background

The northeast Indian region presents a complex tectonic province displaying juxtaposition of two mobile belts, the E–W trending Himalaya and the N–S trending Arakan Yoma belt developed as a consequence of collision between the Indian and the Eurasian plates, and the underthrusting of the Indian plate below the Myanmar plate, respectively (Dasgupta et al. 2000). The major background tectonic setup can be divided into the eastern (or upper) Himalaya structures, the Mishmi massif, the Indo Myanmar arc, the Brahmaputra valley, and the Shillong plateau (Nandy 2001).

The Himalayan structures comprise of thrust planes namely Main Central Thrust (MCT), Main Boundary thrust (MBT), Main Frontal Thrust (MFT), and their subsidiary thrusts. The Mishmi region traversed by Mishmi thrust, Lohit thrust, Po Chu fault, and Tidding suture forms a prominent tectonic intricacy. The major structures also include the Tsangpo suture, Tuting and Bame faults. A conjugate set of faults is also found in the zone namely, right lateral NW–SE trending Po Chu Fault and a left lateral NE–SW trending fault parallel to the Bame fault. The Shillong plateau is characterized by a number of faults, shear and lineaments – the major ones being the N–S trending Dhansiri and Kulsi faults, N–E trending Barapani Shear Zone, and several NE–SW and N–S trending lineaments. Other features include Mikir Hills, Dhubri, Sylhet and Duaki faults, and Dudhnai and Kulsi faults. The Mikir hill is detached from the Shillong plateau by the NW–SE trending Kopili and on the north by Dhansiri fault. The Assam valley zone or the Brahmaputra basin lies on the northern territory edged by the NE–SW trending Naga thrust on the southeastern flank. The Kopili fault is etched on the middle of the Brahmaputra basin followed by Bomdila lineament on the northwest. Disang thrust is seen southeast to the Kopili fault and adjacent to the Naga thrust. On the southern part of the study region, structures predominant are the regional antiforms and synforms with the N–S trending axes, and the N–E and N–W trending conjugate fault/lineament system developed as a result of E–W compression. The N–S trending Tripura-Cachar fold belt constitutes a different tectonic domain. The Indo Myanmar arc, sidelined by Patkoi–Naga–Manipur–Chin hills, is manifested by the Arakan Yoma range to form the Eastern Boundary Thrust (EBT). An oblique subduction is said to occur in the arc. EBT zone is demarcated on the east by the Shan Sagaing fault. High angle reverse fault parallel to the regional N–S folds dominates in the eastern part of the outer arc ridge in the zone. The Arakan Yoma range has been observed with fault plane solutions of deep focus earthquakes in Indo-Myanmar arc indicating thrust mechanisms.

A few notable earthquakes in the region as listed in Table 1 present the seismotectonic implications of the region. The Cachar earthquake of 1869 is believed to have occurred on the Kopili fault. Bilham and England (2001) associates the Great Earthquake of 1897 with the ‘pop-up’ tectonics between the Dauki fault and the Oldham fault in the Shillong plateau. The Great Earthquake of 1950 is believed to have originated from right lateral shear movement along the Po Chu fault (Ben-Menahem et al. 1974). The Srimangal Earthquake is associated with the Sylhet

Table 1 List of some notable earthquakes in the northeast Indian region

Place	Date	Magnitude	Description
Cachar	Jan 10, 1869	M_W 7.4	Damage of Buildings, land fissures, liquefaction and sand venting
Shillong	Jun 12, 1897	M_W 8.1	Devastation of Shillong, more than 1600 fatalities
Assam	Aug 15, 1950	M_W 8.6[a], M_W 8.7[b]	Wide spread devastations in the region. Fatalities reported about 1,526
Srimangal	Jul 08, 1918	M_S 7.6	Damage of buildings
Dhubri	Jul 02, 1930	M_S 7.1	Damage to old constructions, however no loss of life reported
Manipur	Aug 06, 1988	M_w 7.2	The entire region shook

[a] Kanamori (1977)

[b] The present study

and N–W trending Mat faults, and the Dhubri earthquake of 1930 with the Dhubri fault while the Manipur Earthquake of 1988 occurred on the Indo Myanmar Arc.

3 Earthquake database

Recent study by Scordilis (2006) exhibited that on a global scale, earthquake magnitudes estimated by National Earthquake Information Center (NEIC; http://neic.usgs.gov/neis/epic/) and International Seismological Center (ISC) catalogues are practically equivalent. The ISC catalogue has been accredited with higher annual earthquake volume compared to any other global catalogues (Willemann and Storchak 2001). Therefore, the preliminary data catalogue intended for the present analysis is derived from the ISC catalogue accessible at http://www.isc.ac.uk/bull (last accessed February 2007; ISC 2007) covering a period 1906–2006, and the entire study region and the vicinity bounded within the latitude–longitude: 19°N 85°E and 32°N 101°E.

A major issue with earthquake catalogues is the use of different magnitude scales. As such the size of earthquakes is usually defined by magnitudes. Different types of magnitude scales exist mostly due to numerous combinations of wave types and recording instruments. Local magnitude, M_L, was defined by Richter (1935) on the basis of the trace amplitudes of earthquakes by Wood–Anderson seismographs. On the other hand, the body-wave magnitude, m_b, is based on the ground amplitude of body waves with a period of about 1s recorded at long distances and the surface wave magnitude, M_S, is based on the ground amplitude of surface waves with a period of about 20s at distances between 15° and 130° (Gutenberg 1945a, b). The relationship between M_S and M_L as given by Gutenberg and Richter (1956) is

$$M_S = 1.27(M_L - 1) - 0.016M_L^2. \quad (1)$$

M_L, M_S and m_b scales saturate at different levels for large earthquakes, and do not behave uniformly for all magnitude ranges often resulting in incorrect estimation of earthquake magnitude. These limitations are overcome with the moment magnitude, M_W, which is based on the scalar seismic moment, M_0 (Kanamori 1977). Theoretically, the reliability of the scale is ascribed by the fault size and the dislocation associated with the seismic moment. M_W is defined by Hanks and Kanamori (1979) as

$$M_W = \frac{2}{3}\log_{10}M_0 - 6.05 \quad (2)$$

where M_0 is the scalar seismic moment in Nm. The homogenization of earthquake catalogue involves expressing the earthquake magnitudes in one common scale. Practical problems, such as seismic hazard assessment, necessitate use of homogenized catalogue. As such a consistent magnitude should be used for investigating the frequency magnitude distribution (FMD). Pertinently, M_W is preferred because of its applicability for all ranges of earthquakes; large or small, far or near, shallow or deep focused.

Several magnitude scales are used in the ISC catalogue of which the body wave magnitude $m_{b,ISC}$, the surface wave magnitude $M_{S,ISC}$ and local magnitude $M_{L,ISC}$ are predominant. Acronym specifying the data source is added as an additional subscript to the usual definition of the magnitude scales for ease of identification.

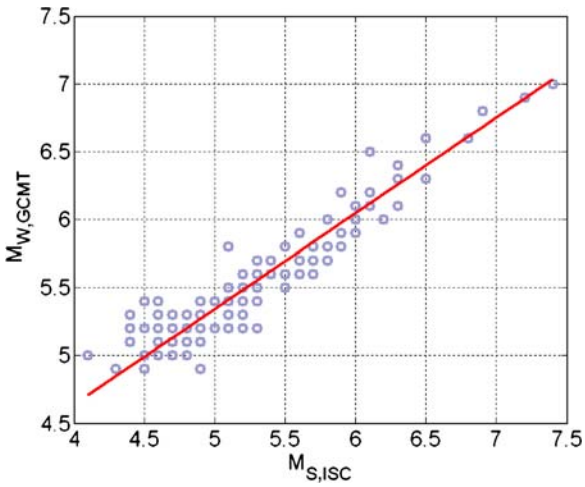

Fig. 1 Correlation of $M_{W,GCMT}$ with $M_{S,ISC}$ from 121 events in the study region

Global Centroid Moment Tensor (GCMT) database at http://www.globalcmt.org (last accessed February 2007) formerly known as the Harvard CMT catalogue provides earthquake data in scalar seismic moment. Kagan (2003) places the accuracy of moment magnitude in the database with an uncertainty in the order of 0.05–0.09, depending on the focal depth, time and magnitude. The database is found to have 130 entries covering the region for the period from 1976 to 2006. However, only three events designated by $M_{W,ISC}$ could be connected to the database.

A homogenous catalogue in M_W can be constructed using the empirical relationships between M_W, M_S, m_b and M_L established by correlating the entries for the same earthquakes in the catalogues derived from the ISC catalogue as well as the GCMT database for the region (e.g. Bormann et al. 2007; Stromeyer et al. 2004). Orthogonal regression (OR) rather than the conventionally followed standard linear least square method has been demonstrated to be more appropriate for magnitude scale regressions (Castellaro et al. 2006). Accordingly, generalized orthogonal regression (GOR) is performed in the present analysis. GOR employs an error variance ratio, denoted by 'η', between the error variances of the linearly related variables on vertical and horizontal axis, respectively. Assuming a case of $\eta = 1$ may not be practical since considerable disparity is found in the accuracies of magnitudes reported by different catalogues (Kagan 2003). In the present analysis, the comparative standard deviation associated with different magnitude scales is placed to be 0.15, 0.20 and 0.25 for $M_{W,GCMT}$, $M_{S,ISC}$ and $m_{b,ISC}$, respectively. These values are roughly estimated from the standard deviations of the magnitude differences between same entries in both the data sources for the respective magnitude scales, and are also more or less comparable with those estimated by Castellaro et al. (2006) for the events recorded in Italy.

The correlation of $M_{W,GCMT}$ and $M_{S,ISC}$ from 121 entries as depicted in Fig. 1 is seen to follow the relation,

$$\begin{aligned} M_{W,GCMT} &= 0.7042(\pm 0.0356)\, M_{S,ISC} \\ &\quad +1.8197(\pm 0.1896), \\ &\quad \text{for } M_{S,ISC} < 7.5,\ n = 121 \end{aligned} \tag{3}$$

Similarly, the regression between $M_{W,GCMT}$ and $m_{b,ISC}$ as presented in Fig. 2 yield the following relation,

$$\begin{aligned} M_{W,GCMT} &= 1.3691(\pm 0.211)\, m_{b,ISC} \\ &\quad - 1.7742(\pm 1.139), \\ &\quad \text{for } M_{W,GCMT} > 4.4,\ m_{b,ISC} < 6.7,\ n = 30 \end{aligned} \tag{4}$$

Equation 2 is seen to have significant dispersions, and hence is not preferred in the present analysis. As such non-linearity is often found in the correlation between M_W and m_b that implicates high conversion errors

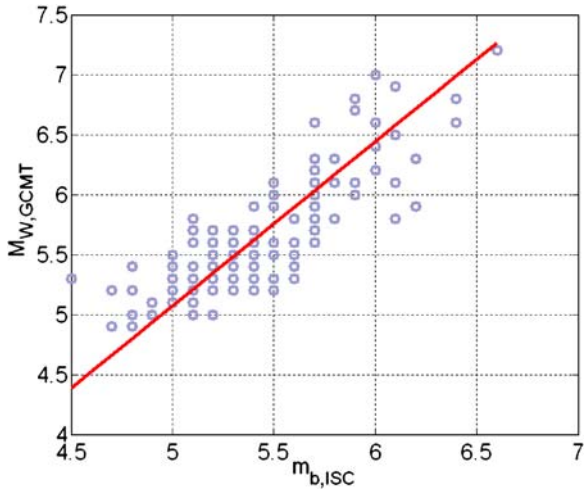

Fig. 2 Correlation between $M_{W,GCMT}$ and $m_{b,ISC}$ for 130 earthquakes that occurred in the study region during 1976 to 2006 in the study region

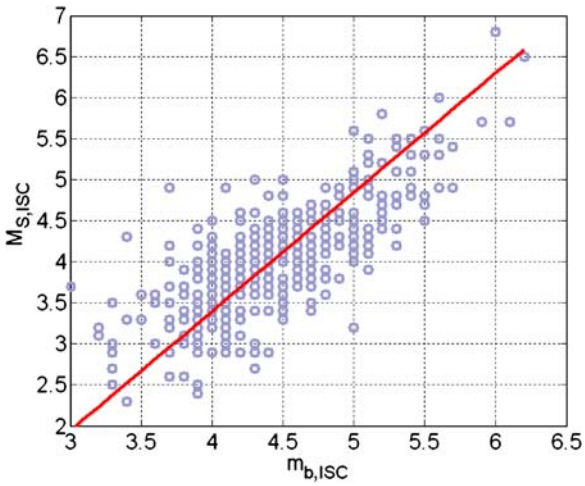

Fig. 3 Correlation of $m_{b,\ ISC}$ with $M_{S,\ ISC}$ from 469 events in the study region

(Castellaro et al. 2006). Furthermore, the correlation of $m_{b,ISC}$ with $M_{S,ISC}$ from 469 entries as depicted in Fig. 3 is found to follow the relation,

$$M_{S,ISC} = 1.4511(\pm 0.0419)m_{b,ISC} - 2.4101(\pm 0.1851), \text{ for } m_{b,ISC} < 6.3,\ n = 469 \quad (5)$$

The number of points correlating $m_{b,ISC}$ and $M_{S,ISC}$ is seen to be scanty at the higher magnitudes, which conforms to the saturation of the body wave magnitude scale at higher magnitude ($m_b > 6$; Kanamori 1983).

However, the data to correlate $M_{W,GCMT}$ and $M_{L,\ ISC}$ is found to be scanty, and largely scattered ruling out a suitable model fit. In a previous study by Heaton et al. (1986), M_L and M_W were shown to be roughly equivalent up to magnitude 6.0. Deichmann (2006) also pointed out theoretically that M_L and M_W are equivalent over the entire range for which M_L can be determined. Furthermore, Ristau et al. (2005) reported that in the western Canadian region, the continental crust events (as is the case with the present study) indicated $M_W = M_L$ for earthquakes with $M_L \geq 3.6$. From these considerations and observations, M_L is assumed almost equivalent to M_W in the present analysis. Nevertheless, it should be noted that the procedure to determine M_L depends on the recording seismographs, which imply observational differences in different cases and hence implicates that the appropriate region specific relationships be derived by analyzing relevant waveform data (e.g. Braunmiller et al. 2005) in a future study.

Equation 1 is employed to obtain M_W equivalent for the M_S entries extending up to M_W 7.6. On the other hand, the m_b entries in the catalogue have been scaled to M_S and subsequently to M_W through Eqs. 1 and 2. Furthermore, those entries not under the provision of the given relationships are taken care of by connecting to entries in other catalogues on one-to-one correspondence. The maximum magnitudes reported in the catalogue is 6.6 in $m_{b,ISC}$, 5.0 in $M_{L,\ ISC}$, and 8.7 in $M_{S,ISC}$. Four entries in the catalogue have $m_{b,ISC}$ values >6.2 as listed in Table 2, for which scaling by Eq. 3 is not applicable. For the events of the years 1988 and 1995, the corresponding M_W values are obtained from GCMT database. The 1970 event is assigned M_W 6.8 correlating with that of the event on August 20, 1988. The largest earthquake reported in the catalogue is the Great Assam Earthquake of 1950, M_S 8.6. Kanamori (1977) placed it as M_W 8.6. Brune and Engen (1969) assigned a seismic moment of 4.31×10^{21}Nm to this earthquake. However, later workers associated high value of seismic moment to the tune of 21.0×10^{21}Nm (Ben-Menahem et al. 1974) and 9.5×10^{21}Nm (Chen and Molnar 1977). The average magnitude computed with the later values from the seismic moment magnitude relation (Hanks and Kanamori 1979) would be M_W 8.715 implicating a value of M_W 8.7 to the earthquake in this study. The Great Nepal-Bihar Earthquake of 1934 in the central Himalaya with M_S 8.3 lies on the western margin of the region, and is beyond the spatial scope of the present study since our focus is on the eastern and northeastern Himalaya. The earthquake of 1951 with M_S 8.0 is connected with M_W 7.8 correlating with the one in the Chinese catalogue (Rong 2002). Three shallow earthquakes ($M_S > 7.6$) reported in the ISC catalogue and not connected to any equivalent value in M_W–1912/05/23 M_S 8.0, 1946/09/12 M_S 7.8, and 1947/07/29 M_S 7.7 are assumed practically equivalent to M_W values.

A time series of the number of events against each year is shown in Fig. 4. Number of events against hour of the day plot as depicted in Fig. 5a does not indicate any significant extraneous recordings that could occur due to contamination from explosions. On the other hand, the depth distribution from the catalogue as shown in Fig. 5b exhibits extraneously higher number at 33km depth implying that those depth records are not reliable for the earthquake depth analysis. Furthermore, depths

Table 2 The list of earthquake with $m_{b,\ ISC}$ >6.2 in the catalogue during 1964 to 2006 with the corresponding M_W

Date	Time	Lat (°N)	Lon (°E)	Depth (km)	$m_{b,ISC}$	M_W
1970/07/29	10:16:20.40	26.0200	95.3700	68.0	6.4	6.8
1988/08/06	00:36:25.54	25.1297	95.1493	100.1	6.6	7.2
1988/08/20	23:09:10.14	26.7198	86.6261	64.6	6.4	6.8
1995/05/06	01:59:07.04	24.9605	95.2949	117.6	6.3	6.4

reported ≥250km are associated with rather high standard deviations. The entries indicate that shallow earthquakes (<70km) are dominant in the region. However, intermediate depth earthquakes (70–300 km) are mostly concentrated in the Arakan Yoma range in the Eastern Boundary Thrust region, albeit sparsely distributed over the remaining region. A seismotectonic map prepared with the data catalogue is presented in Fig. 6.

4 Seismicity analysis

A quantitative approach to seismicity analysis can be carried out with the assessment of seismicity parameters: a and b value, and correlation fractal dimension, D_C. The first two parameters are obtained from FMD given by Gutenberg-Richter (GR) relation. The relation as given by Gutenberg and Richter (1944) is,

$$\log_{10} N = a - \mathrm{bm}, \tag{6}$$

where N is the cumulative frequency of occurrence of magnitude m in a given earthquake database. The intercept and slope, a and b value, respectively, signify the background seismicity level, and the magnitude size distribution.

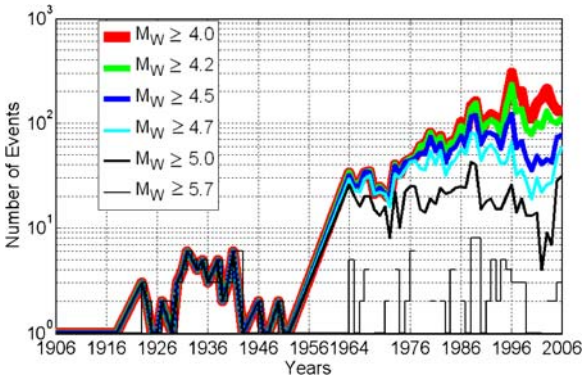

Fig. 4 A time series of events in the catalogue indicates significant and stable recording from 1964 onwards. However the recording of events with magnitude >5.6 is seen to be reasonably stable from 1924 onwards

5 The *b* value and correlation fractal dimension

In several studies, b value has been found to vary both spatially and temporally, and has often been employed as one parameter approach for seismicity analysis. A low b value implies that majority of earthquakes are

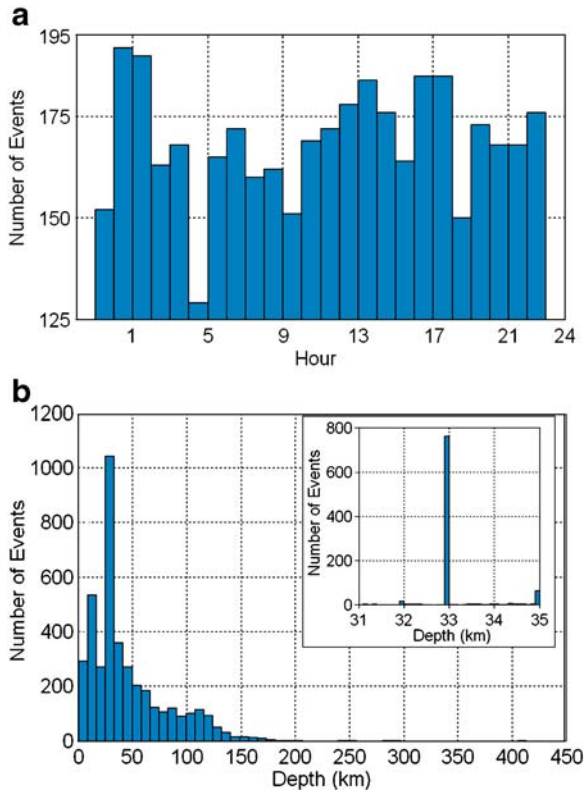

Fig. 5 **a** Number of events against hour of the day plot shows overall consistency of number of events from a low of 129 to high of 192, but mostly between 150 and 175 indicating no significant extraneous recording. **b** Depth distribution from the catalogue shows extraneously high number at around 33 km depth; most likely due to software used for depth calculation that constrains the lower limit to 33 km

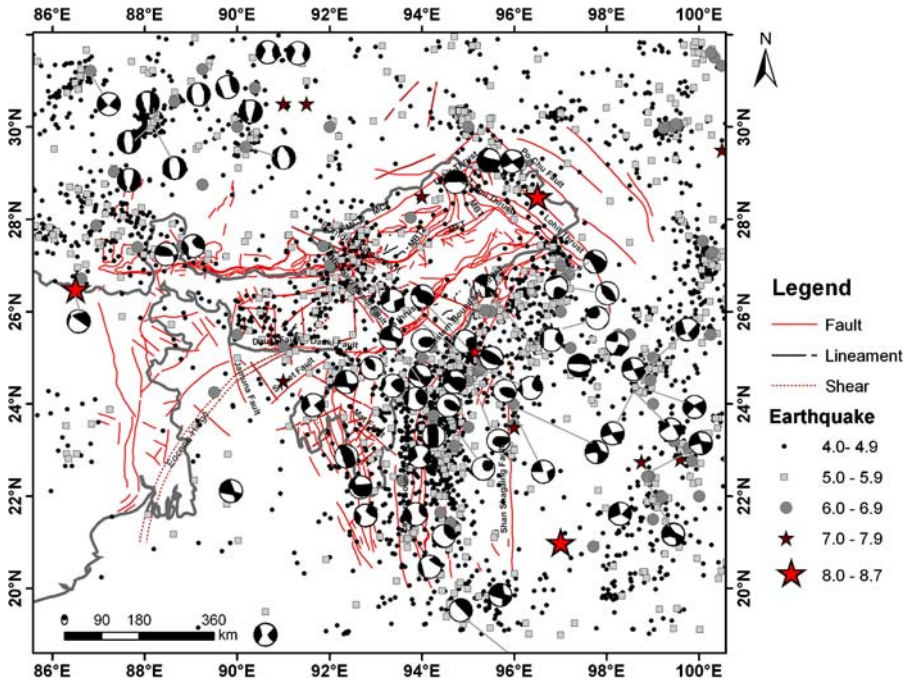

Fig. 6 A seismotectonic map of northeast India and its adjoining region prepared with the earthquakes from the data catalogue of the present study. The tectonic features are adapted from Dasgupta et al. (2000) while the beach balls are taken from GCMT database for the earthquakes of M_W>5.4 covering a period from 1976 to 2006

of higher magnitude, and a high b value implies that the majority of earthquakes are of lower magnitude. The variation of b value has been seen to be inversely related to stress distribution (Mogi 1962; Wesnouski et al. 1983; Schorlemmer et al. 2005). Furthermore, large material heterogeneities have been reported with higher b values (Scholz 1968). Aftershocks have been reported to have high b values while foreshocks have been associated with low b values (Suyehiro et al. 1964; Nuannin et al. 2005). In spatial analysis, low b value can be inferred as growing stress regime unleashing larger magnitude earthquakes while high b value indicates low stress buildup with continued stress release through numerous smaller magnitude earthquakes.

The estimation of b value is generally performed by maximum-likelihood method (Aki 1965; Bender 1983; Utsu 1999) given as,

$$b = \frac{\log_{10}(e)}{\left[m_{mean} - \left(m_t - \frac{\Delta m}{2}\right)\right]}, \quad (7)$$

where m_{mean} is the average magnitude and Δm is the magnitude bin size. Schorlemmer et al. (2003) suggests a bootstrap method (Chernick 1999) to estimate the associated standard deviation, δb, of b value. The approach involves computation of b value repeatedly for a number of times, each time employing different replacement events drawn from the associated catalogue wherein any event can be selected more than once. The error is, then, estimated as the standard deviation associated with the computed values.

Another commonly used seismicity parameter is the fractal correlation dimension of earthquakes, D_C. The parameter is implied as a power law exponent relating distance and the number of pair of points of either epicenters or foci within the distance (Kagan 2007). The temporal variations in the fractal dimension can enable assessment of seismic processes (Kagan and Knopoff 1980). A lower D_C value indicates higher clustering while a higher D_C value implies uniform or random spatial distribution. D_C has been implicated as a quantifier of crustal deformation in time and space (Turcotte 1986). However, the variation of fractal dimension in different seismic zones has also been attributed to the Geological diversity (Aviles et al. 1987). An estimation of D_C can be achieved through correlation

integral method (Grassberger and Procaccia 1983). The fractal correlation dimension is given as,

$$D_C = \lim_{r\to 0} \frac{\log_{10} C(N,r)}{\log_{10}(r)} \quad (8)$$

where

$$C(N,r) = \frac{2}{N(N-1)} \sum_{i=1}^{N} \sum_{j=i+1}^{N} H\left(r - |y_i - y_j|\right). \quad (9)$$

$C(N, r)$ is referred to as the correlation integral. $H(x)$ is Heaviside step function, whose value is 0 if $x < 0$, otherwise 1. N is the total number of points in the query. The coordinates of the location of points are given by y_i and y_j. Essentially, $C(N, r)$ accounts for the number of points that are at a distance ≤r with respect to the total number of pairs of all the points.

A plot of $\log_{10}(C(N, r))$ against $\log_{10}(r)$ is used to estimate D_C as the slope of the curve in its linear bound for a specific range of r. In case of an infinite two-dimensional distribution of epicenters, the plot is a straight line. But practically for larger values of r a state of saturation is attained thereby decreasing the gradient. For smaller values of r, an increase in the gradient is induced indicating a state of depopulation (Narenberg and Essex 1990). The specific range of r is, therefore, projected from the bounds of saturation and depopulation limits.

The two parameters, b value and D_C have been employed together in several studies. The results of Hirata (1989a), Henderson et al. (1992), and Barton et al. (1999) indicated that the two parameters tend to correlate negatively. Oncel and Wilson (2002) also reported the correlations to be generally negative, although both positive and negative correlations could be transiently observed. The correlations are seen to be dependent on the modes of failure within the active fault complex. Wyss et al. (2004) purposed that heterogeneity of seismogenic volumes leads to variations in D_C and b values, and indicated a positive correlation between the two parameters dominant in regions of creeping and locked patches as well. Nonetheless, conclusively D_C and b value together form a composite indicator of the underlying dynamics of the region. The spatial correlations can be interpreted from individual inferences of the variations of D_C and b value. Low values indicate clustering of mainly large earthquakes identifying regions of high stress concentrations. High values suggest random occurrence of mainly smaller earthquakes indicating low stress buildup. Low D_C and high b value indicates clustering of mainly smaller earthquakes that may be implicated with creeping parts of the fault zones. High D_C and low b value indicates random occurrence of mostly larger earthquakes suggesting formation of asperities across the underlying faults (Oncel and Wyss 2000). The spatial variations of both parameters in conjunction can be related to the tectonic dynamics across a region.

6 Methodology

The deployment of seismographs besides the techniques of analysis usually progresses with time leading to decrease of the minimum magnitude of completeness, m_t. Therefore, two important aspects in the catalogue based analysis, besides the data homogeneity, are the starting time of good quality records, and m_t. The value of m_t varies with time and space mainly owing to spatial and temporal irregularities of seismic recording networks. In the present study, the recordings of events are seen to be stable and significant from 1964 onwards as shown in Fig. 4. Hence, a sub-catalogue covering the period from 1964 to 2006 with a reduced spatial bounds of 86°N to 100°N longitudes and 19°E to 31°E latitudes is employed for the analysis.

The constraining parameter, m_t is estimated with the methodology described by Wiemer and Wyss (2000) that assumes power law fit as best fit for FMD at 90% confidence level. The b and a values are estimated as a function of minimum magnitude through Eqs. 7 and 6, respectively, considering only those events with $m \geq m_i$ where m_i is a contender for m_t. The bootstrap method is employed to evaluate the standard deviation of b value, wherein for each case the b values are computed 1,000 times. Thereafter, a predicted distribution of magnitudes is calculated for each b and a values. Subsequently, residual percentage is obtained from the following,

$$\%\text{residual} = \frac{\sum_{m_i}^{M_{\max}} \left| N_i^{\text{obs}} - N_i^{\text{pred}} \right|}{\sum_i N_i^{\text{obs}}} \times 100, \quad (10)$$

where N_i^{obs} and N_i^{pred} are the observed and predicted cumulative number of events in each magnitude bin.

The m_t is defined as the point at which the GR law can model the FMD with residuals under 10%. The entire sub-catalogue is considered to provide an illustration. Figure 7 shows variation of b value with the minimum magnitude as well as the % residual, which goes under 10 at M_W 4.5. A FMD plot for the sub-catalogue, shown in Fig. 8, also indicates a deviation from the linear fit at M_W 4.5 on the lower magnitude range. The associated a and b value are found to be 7.47 and 0.97(±0.017), respectively.

The spatial coverage in the estimation of seismicity parameters is achieved by rolling a square window covering the entire region with a slide of 0.5 degree every time. The b value and D_C are estimated from the events encapsulated by the window only if at least 50 events within the m_t can be employed. The 50 events' criterion is important to achieve a meaningful statistical analysis (Utsu 1965). The estimates are thereafter assigned to the centroid of the window. Adequate spatial coverage is found achievable through a 3° × 3° window, and hence, is adopted for the spatial analysis. Great circle distances between the epicenter positions are used in the estimation of D_C. An estimation of D_C at 87.5°E, 29.5°N is presented in Fig. 9.

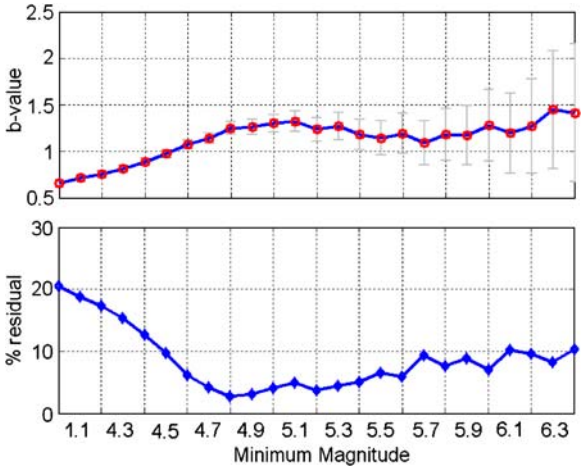

Fig. 7 The variation of b value estimated from GR law fit on the frequency magnitude distribution with minimum magnitude is depicted. The goodness of fit is examined with percent residual estimated by percentage of the residual (i.e. absolute difference of observed and predicted values) over the observed value. The value of m_t is seen to be M_W 4.5 corresponding to b value of 0.97 at % residual ≤10

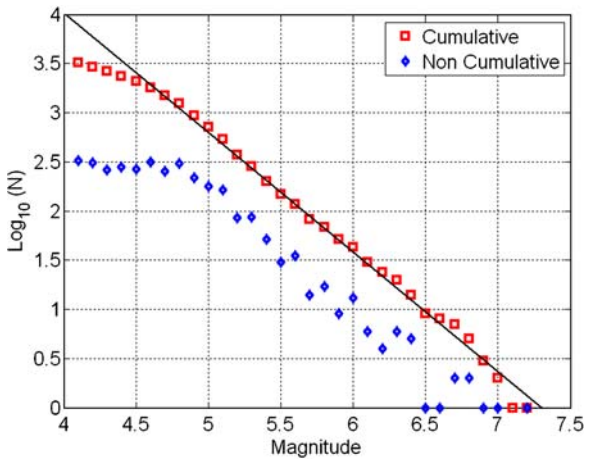

Fig. 8 FMD plot for the entire sub-catalogue shows departure from the linearity on the lower magnitude at M_W 4.5

7 The spatial distributions of seismicity parameters

Spatial analyses essentially capture average characteristics of seismicity parameters over a stipulated time span. The windowing technique employed in the present study highlights the disparity of the estimated parameters across the study region, although constraints by m_t as well as on the number of events introduce considerable spatial gaps in the estimation process. The process accomplished in the present

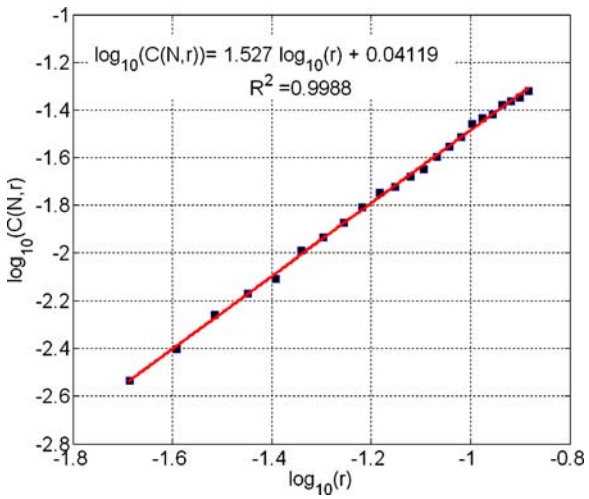

Fig. 9 The estimation of D_C corresponding to the 3°×3° square window with centroid at 87.5°E, 29.5°N from the slope of best fit line on the plot of $\log_{10}(C(N, r))$ against $\log_{10}(r)$. The scale 'r' is measured in degrees

analyses relegates to spatial recording patterns and adequate seismicity adhered to the GR law.

The magnitude of completeness, m_t, is seen to vary from M_W 4.0 to 4.8 across the region as depicted in Fig. 10. Most parts of the region are predominantly associated with m_t~ M_W 4.4–4.5 except in the Shillong plateau region, areas of MBT and MCT, and Lohit thrust zone in the north of EBT where higher values are observed. However, the lower values are attached to Tripura-Cachar fold belt region, and to southeast of the study region.

Spatial distribution of a value goes from a low of 4.47 to as high as 8.59 as shown in Fig. 11. Higher values (≥6.87) are seen in the Shillong plateau area, Mishmi region, northern flank of the eastern Himalaya, and the southern area of EBT. The remaining areas of the study region are observed with moderate to lower values, especially low in the Tripura-Cachar fold belt zone, and southeast of the study region.

The b value distribution as depicted in Fig. 12 ranges from 0.61 to 1.36. The values <1.05 are seen in most of the parts of the study region. The Naga thrust zone, northern EBT, Tripura-Cachar fold belt zone as well as eastern part of the study region are seen with b value <0.9. Higher values, on the other hand, are observed predominantly in the regions of eastern Himalaya, Mishmi, and southern EBT. The spatial variation of δb as depicted in Fig. 13 exhibits a range from 0.032 to 0.146 and is seen mostly positively correlated to the b value distribution. However, the ranges of δb are comparatively low in the southern portion of EBT, and in upper Himalaya vis-à-vis high b values, confirming the observed higher b values. To a large extent, the spatial distributions of m_t, a and b value are seen to follow similar trends.

The fractal correlation dimension, D_C, is found to vary from 0.70 to 1.66 as shown in Fig. 14. By and large, higher values of D_C dominate the study region, indicating that the earthquake epicenters are mostly scattered within their relevant spatial bounds. Furthermore, an overall negative correlation with b value distribution is implicated. The stress build-up is apparently indicated with low b value in the Naga thrust area, northern EBT zone, and the eastern flank of the study region. The correlation of b value and D_C in the regions suggests a case of widening asperity across the underlying faults with scattered higher magnitude earthquakes. However, a trend of positive correlations is emphasized towards the southern EBT with high b values. Similarly, tendency towards the north in the Mishmi region is that of positive correlations with high b values, indicating dispersed seismicity with mostly low magnitude earthquakes. Nevertheless, a slight tendency of negative correlation

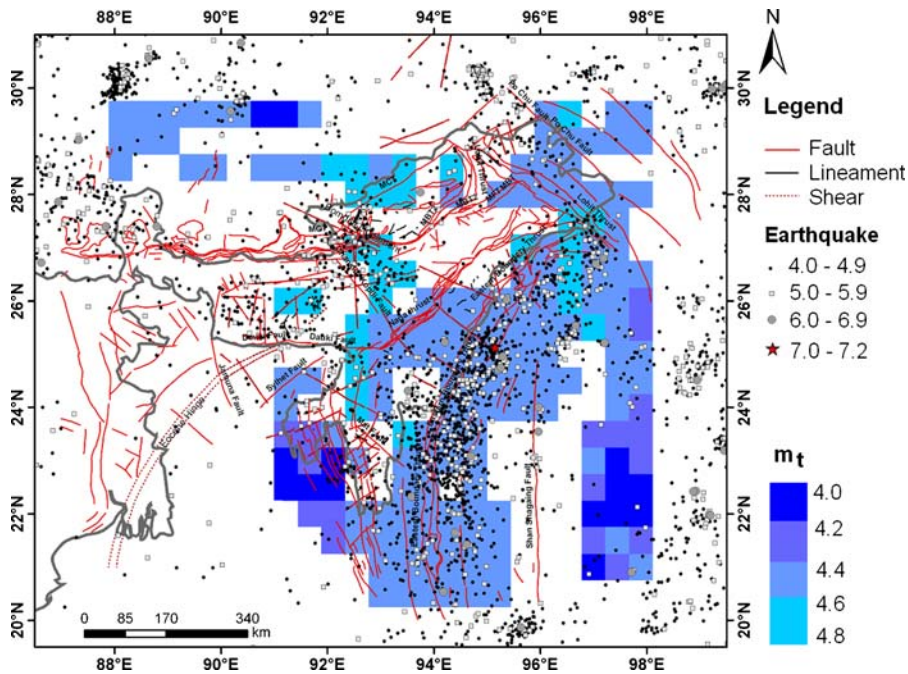

Fig. 10 The spatial distribution of estimated magnitude of completeness or the threshold magnitude, m_t on the backdrop of seismicity with M_W ≥4.0 from the subcatalogue covering a recording period from 1964 to 2006

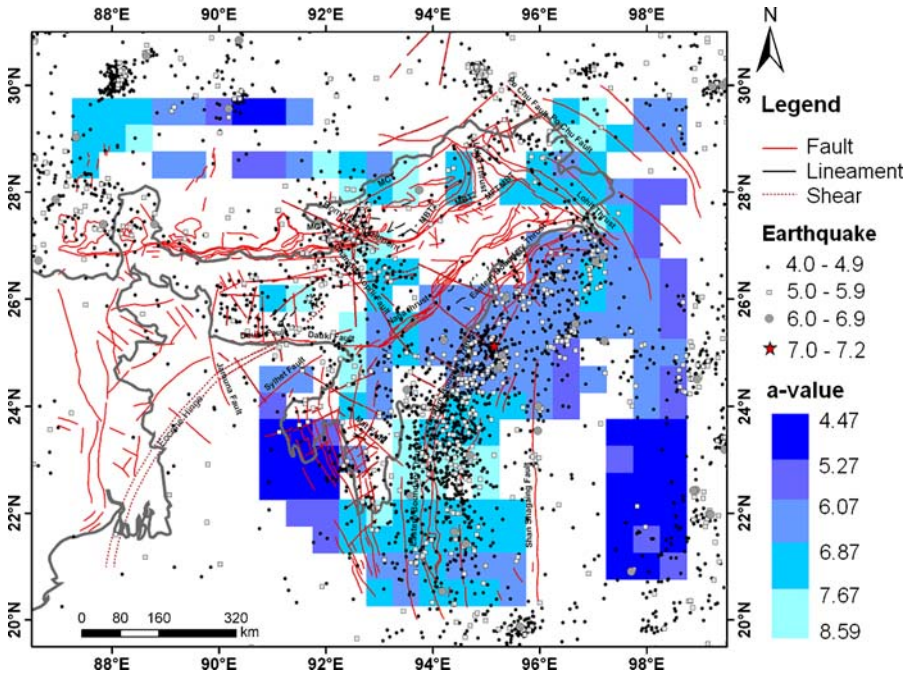

Fig. 11 The spatial distribution of computed *a* value on the backdrop of seismicity with $M_W \geq 4.0$ from the sub-catalogue covering a recording period from 1964 to 2006

is observed to the east of the region with decrease in *b* values. Lower values (D_C <1.2) are observed in the zones of Shillong plateau, MBT and MCT, eastern Himalaya, Tripura-Cachar fold belt and some areas of Mishmi block to the east suggesting clustering of epicenters of higher magnitude earthquakes exhibiting negative correlation. Whereas the trend on the southern flank of Shillong Plateau is of positive correlations – high D_C and high *b* values suggesting scattered low magnitude seismicity. A demarcation

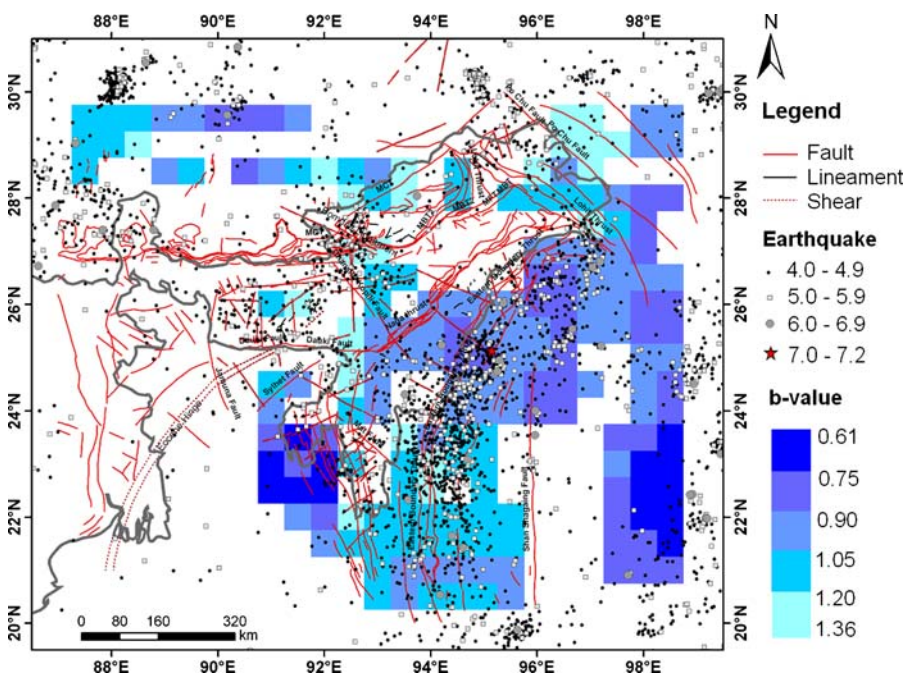

Fig. 12 The spatial distribution of computed *b* value on the backdrop of seismicity with $M_W \geq 4.0$ from the sub-catalogue covering a recording period from 1964 to 2006

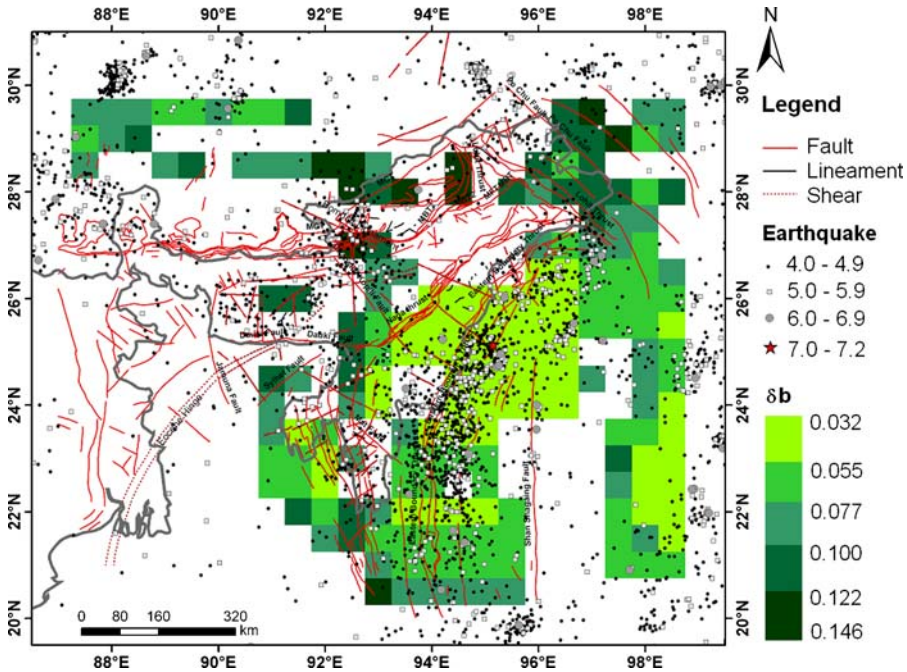

Fig. 13 The spatial distribution of standard deviation of b value (δb) on the backdrop of seismicity with $M_W \geq 4.0$ from the subcatalogue covering a recording period from 1964 to 2006

can thus be observed in the Mat fault zone adjacent to EBT, which indicates scattered low magnitude seismicity to the southeast while areas to the west of the fault in the Tripura-Cachar fold belt is indicated with likely asperity progress related to clustering of higher magnitude earthquakes. On the other hand, in the upper Himalaya, mostly on the northwest of the study region, the clustering phenomenon and the magnitude distributions are observed to be following predominantly positive associations.

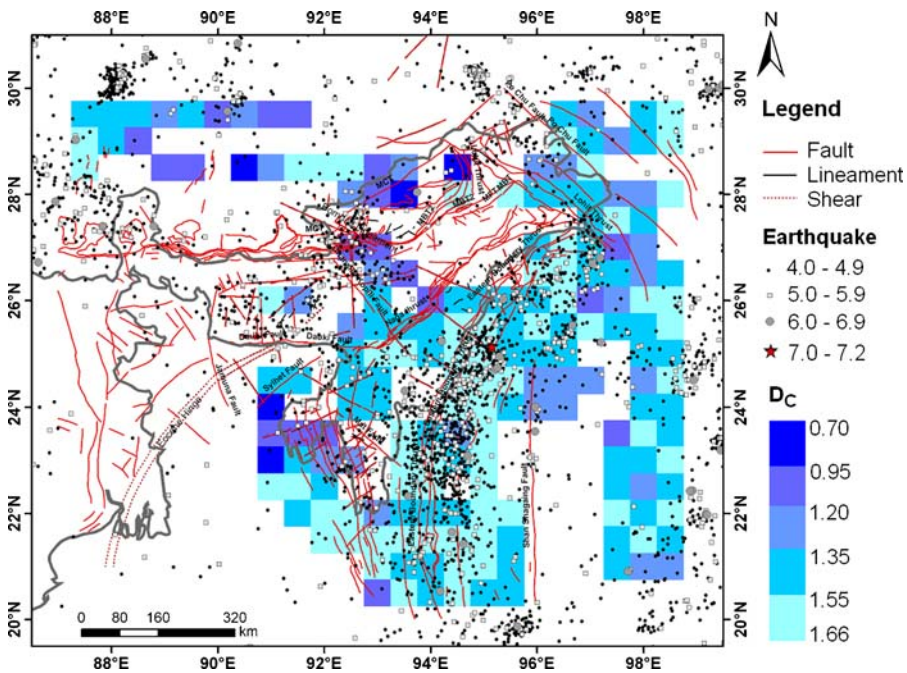

Fig. 14 The spatial distribution of correlation fractal dimension, D_C on the backdrop of seismicity with $M_W \geq 4.0$ from the subcatalogue covering the recording period from 1964 to 2006

The zonation of seismicity parameters identifies most of the study region as highly seismic with frequency magnitude distribution indicating dominance of higher magnitude earthquakes, and the spatial occurrence mostly scattered across the region.

8 Fractal dimension of fault segments

The seismicity of a region is mostly rendered by the underlying active fault network as the earthquakes generally nucleate from within the faults. A quantitative study of the fault system is, therefore, important to appreciate the underlying geodynamic regime of the earthquake occurrence. Fracturing or the fractal geometry of the fault system can be quantified through box counting estimated fractal dimension (Hirata 1989b). The fractal dimension of a fault segment, D is computed by dividing the square area of length R enclosing the system into regular square grid of boxes of length r. If the fault system has a self similarity structure, then

$$N(r) \sim r^{-D} \tag{11}$$

where $N(r)$ is the number of boxes that the fault line enters and D is a fractal dimension or more specifically a capacity dimension (Mandelbrot 1983). D is referred to as box-counting estimated fractal dimension, and is assessed from the slope of the linear fit on the plot between $\log_{10}N(r)$ and $\log_{10}$ r. Equation 11 may be seen valid only for certain range of scales, i.e. range of values of r, within which the self-similarity structure exists.

In the present study, the box counting method is employed to examine the segments of active fault network in the study region. The data employed is a fault map on a digital raster monochrome image covering an area of 87°E to 99°E and 22°N to 30°N as exported from GIS. The image is split into thirty square images, each either enclosing a part or none of the fault system. Thereafter, the box counting algorithm is employed to each image containing the fault structures to compute the pertaining fractal dimension D, which is estimated as the slope of the linear fit on the plot between $\log_{10} N(r)$ against $\log_{10} r$, where $N(r)$ is the number of boxes entered by the fault structure, and r is the number of boxes scaled on one side of the image as shown in Fig. 15. The estimated fractal dimensions represent measure of geometry of the fault systems as the employed fault segments predominantly pertains to major faults active in the region.

The estimated D is found to vary from 1.20 to 1.51. Figures 16a and b depict the estimated D and its estimated standard deviation δD, respectively, for each corresponding segment. A value close to 2 suggests that it is a plane that is being filled up, while a value close to 1 implies that line sources are predominant (Aki 1981). The results corroborate the findings to upper limit of 1.6 as indicated by Hirata (1989b). The Himalayan structures are seen with higher values towards 1.51. The zones of Naga thrust, Lohit thrust, the EBT and that of Mat fault and the south western to it are similarly seen with high D values. The moderate values are observed across the Shillong plateau region and the southern EBT. The standard deviations associated with the estimated fractal dimension of the segments imply that there is no much statistically significant difference in the estimated values over narrow ranges in most of the case. However, low standard deviations as observed with high D values associated with the segments containing the Himalayan structures sustain the estimated high values.

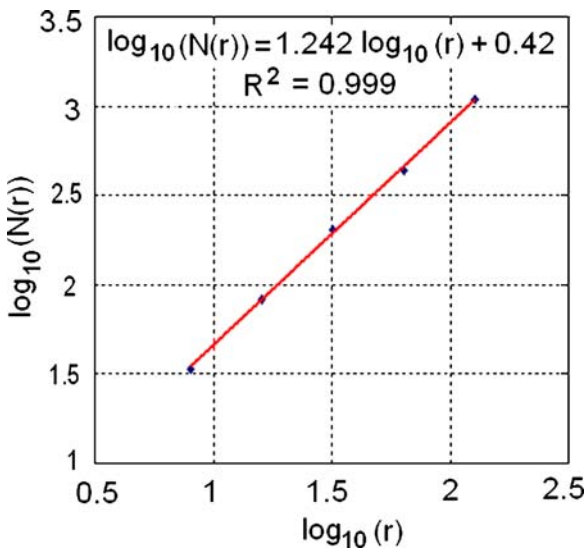

Fig. 15 The estimation of fractal dimension D for the fault segment with the centroid at longitude 88°E and latitude 23°N from the slope of the best fit line on the plot of $\log_{10}(C(N, r))$ against $\log_{10}(r)$. The scale 'r' is the number of square boxes on one side of the entire box

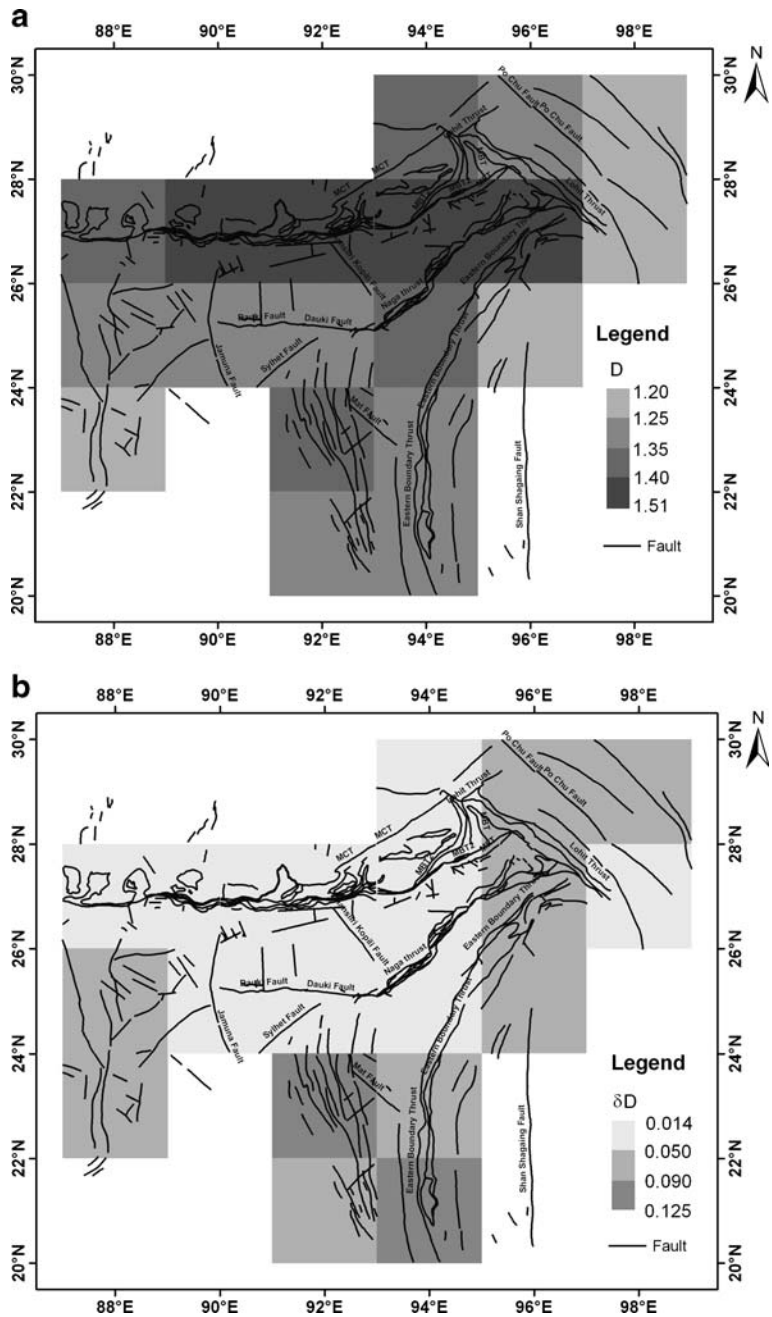

Fig. 16 **a** The spatial zonation of the box-counting estimated fractal dimension, D, for the fault segments. **b** The spatial zonation of the standard deviation, δD, of box counting estimated fractal dimension, D, for the fault segments

9 Source zone classification

Finally, the present study addresses a fundamental task in seismic hazard assessment process –the seismic source zone classification. The seismic source zones are primarily of two types – linear and areal. Linear sources involve identification and classification of active faults. On the hand, areal source zone accommodates unknown subsurface complexities of an active seismic province such as fault systems through applicable spatial scopes. The areal classification is usually achieved by various methods such as establishment of polygons in accordance with Geological, Geophysical, and Seismological data (Thenhaus and Campbell 2003), and the smoothening of spatial seismicity (Woo 1996). In the present study, the

spatial pattern of seismicity quantified by b value and D_C are employed along with the underlying tectonic network. The method involves segregation of varying correlations of b value and D_C in accordance with the fault patterns. Thus, the northeast Indian region is broadly classified into four seismic source zones – Eastern Himalayan Zone (EHZ), Mishmi Block Zone (MBZ), Eastern boundary Zone (EBZ), and Shillong Zone (SHZ) as shown in Fig. 17.

The seismotectonics of the region as displayed in Fig. 6 indicates activities due to thrust, normal and strike slip motions across the region. The beach balls presenting oblique reverse focal mechanism implicates thrusting and is seen to dominate in the northern EBT where earthquake foci are mostly in the intermediate depth (70 < km < 300). However, the southern part of EBT shows significantly strike slip mechanism. The observed trend of focal mechanisms in the zone relates to oblique thrusting in the territory. The strike slip mechanism is also seen on the Mishmi zone of Lohit thrust and Po Chu fault. The zones of Dauki fault and that of Dhansiri Kopila fault in the Shillong Plateau region exhibits strike slip focal mechanisms. On the other hand, the earthquake mechanisms are predominantly normal in the eastern/upper Himalayan region. Accordingly, the EHZ is associated with predominantly normal faulting mechanism with significantly shallow occurring earthquakes. MBZ and SHZ have dominantly strike slip focal mechanism with shallow earthquakes. EBZ on the other hand has predominantly oblique reverse focal mechanism – with the occurrence of intermediate depth earthquakes.

10 Discussion and conclusions

Region specific magnitude scaling relations have been established for the study region, which facilitated the generation of a homogenous earthquake catalogue for the present analysis. The seismicity analysis in the region has been performed with a sub-catalogue (1964–2006), considering the stability and improved earthquake recordings from 1964, which is likely due to the advent of World-Wide Standard Seismographic Network (WWSSN). The analysis highlighted variations of seismicity in the study region, although significant spatial gaps have been found due to either lack of valid minimum magnitude of completeness or inadequate number of events. The spatial patterns of seismicity parameters – m_t, a and b value exhibited by and large positive correlations in the study region.

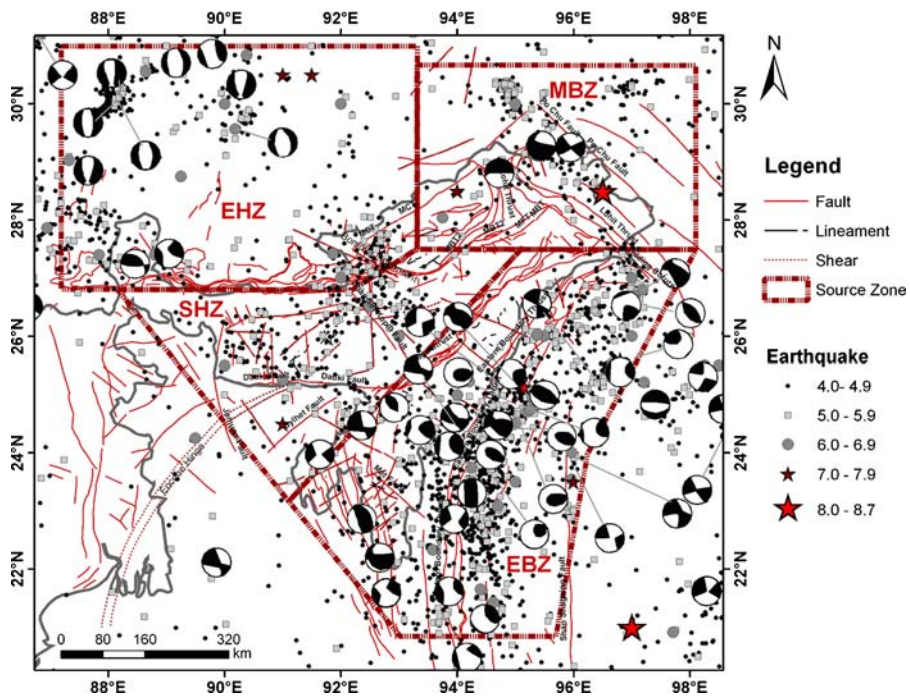

Fig. 17 The classified source zones demarcated by the polygons

The spatial distribution of δb also follows positive correlations with the estimated b values in most of the cases, wherein low b values are seen with low standard deviation indicating an overall tendency of low b values across the study region. To this effect, the lower b values are seen predominant in the thrust zones and moderate to higher values in the zones exhibiting strike slip and normal focal mechanism. The results of the present study are comparable with those of recent works (Scholemmer et al. 2005; Wyss et al. 2004; Oncel and Wilson 2002). Mostly high values of D_C have been seen across the region that exhibits high the box-counting fractal dimension, D, of the underlying predominant fault segments. Negative correlation is quite dominant in the northern EBT and Tripura-Cachar fold belt with low b value, while other regions tend to differ. The trend of moderately high b values on the north and high on the south seem to corroborate oblique reverse faulting mechanism in the northern EBT. However, in Shillong plateau area, the mechanisms of earthquake occurrence are considerably different with higher b values but low D_C. In the eastern Himalaya with predominantly normal faulting mechanisms, positive correlations are exhibited with high b values. Similarly positive correlations are also observed in the Mishmi massif region of Po Chu fault and Lohit thrust exhibiting high b values. Lastly, the established spatial seismicity patterns of b value and D_C with the consideration of underlying active fault networks have been applied to demarcate four broad seismic source zones, designated as EHZ, MBZ, EBZ, and SHZ, in the study region. The analysis of the recent seismicity in the northeast Indian region performed thus accomplishes a basic groundwork towards seismic hazard assessment of this earthquake-prone country of India.

Acknowledgment The critical review and constructive suggestions of the anonymous referee greatly helped in significantly improving the manuscript with enhanced scientific exposition.

References

Aki K (1965) Maximum likelihood estimate of b in the formula log N=a-bM and its confidence limits. Bull Earthq Res Inst Univ Tokyo 43:237–239

Aki K (1981) A probabilistic synthesis of precursor phenomena. In: Simpson DW, Richards PG (eds) Earthquake Prediction, Maurice Ewing Series 4, AGU 566–574

Aviles CA, Scholz CH, Boatwright J (1987) Fractal analysis applied to characteristic segments of the San Andreas fault. J Geophys Res 92:331–344

Barton DJ, Foulger GR, Henderson JR, Julian BR (1999) Frequency-magnitude statistics and spatial correlation dimensions of earthquakes at Long Valley caldera. California. Geophys J Int 138:563–570

Bender B (1983) Maximum likelihood estimation of b values for magnitude grouped data. Bull Seism Soc Am 73:831–851

Ben-Menahem A, Aboodi E, Schild R (1974) The source of the great Assam earthquake–an interplate wedge motion. Phys Earth and Planet Int 9:265–289

Bhatia SC, Ravi Kumar M, Gupta HK (1999) A probabilistic seismic hazard map of India and adjoining regions. Ann di Geofis 42:1153–1166

Bilham R, England P (2001) Plateau ' pop up' in the great 1897 Assam earthquake. Nature 410:806–809

BIS (2002) IS 1893–2002 (Part 1): Indian standard criteria for earthquake resistant design of structures, part 1–general provisions and buildings. Bureau of Indian Standards, New Delhi

Bormann P, Liu R, Ren X, Gutdeutsch R, Kaiser D, Castellaro S (2007) Chinese national network magnitudes, their relation to NEIC magnitudes, and recommendations for new IASPEI magnitude standards. Bull Seism Soc Am 97:114–127

Braunmiller J, Deichmann N, Giardini D, Wiemer S (2005) Homogeneous moment-magnitude calibration in Switzerland. Bull Seism Soc Am 95:58–74

Brune J, Engen G (1969) Excitation of mantle love waves and definition of mantle wave magnitude. Bull Seism Soc Am 57:1355–1365

Castellaro S, Mulargia F, Kagan YY (2006) Regression problems for magnitudes. Geophys J Int 165:913–930

Chen W, Molnar P (1977) Seismic moments of major earthquakes and average rate of slip in Central Asia. J Geophy Res 82:2945–2969

Chernick MR (1999) Bootstrap methods: a practitioner's guide, Wiley Series in Probability and Statistics. Wiley, New York

Dasgupta S, Pande P, Ganguly D, Iqbal Z, Sanyal K, Venaktraman NV, Dasgupta S, Sural B, Harendranath L, Mazumadar K, Sanyal S, Roy A, Das LK, Misra PS, Gupta H (2000) Seismotectonic Atlas of India and its Environs. Geological Survey of India, Calcutta, India

Deichmann N (2006) Local magnitude, a moment revisited. Bull Seism Soc Am 96:1267–1277

Grassberger P, Procaccia I (1983) Measuring the strangeness of strange attractors. Physica D 9:189–208

Gutenberg B (1945a) Amplitudes of surface waves and magnitudes of shallow earthquakes. Bull Seism Soc Am 35:3–12

Gutenberg B (1945b) Magnitude determination for deep-focus earthquakes. Bull Seism Soc Am 35:117–130

Gutenberg B, Richter CF (1944) Frequency of earthquakes in California. Bull Seism Soc Am 34:185–188

Gutenberg B, Richter CF (1956) Magnitude and energy of earthquakes. Ann Geofis 9:1–15

Hanks TC, Kanamori H (1979) A moment magnitude scales. J Geophysis Res 84:2348–2350

Heaton TH, Tajima F, Mori AW (1986) Estimating ground motion using recorded accelerograms. Surv Geophys 8:25–83

Henderson JR, Main IG, Pearce RG, Takeya M (1992) Seismicity in North eastern Brazil: fractal clustering and the evolution of the b value. Geophys J Int 116:217–226

Hirata T (1989a) A correlation between the b value and the fractal dimension of earthquake. J Geophys Res 94:7507–7514

Hirata T (1989b) Fractal dimension of fault systems in Japan: fractal structure in rock fracture geometry at various scales. Pageoph 131:157–170

ISC (2007) On-line Bulletin, http://www.isc.ac.uk/Bull, Internatl. Seis. Cent., Thatcham, United Kingdom

Kagan YY (2003) Accuracy of modern global earthquake catalogs. Phys Earth Planet Inter 135:173–209

Kagan YY (2007) Earthquake spatial distribution: the correlation dimension. Geophys J Int 168:1175–1194

Kagan YY, Knopoff L (1980) Spatial distribution of earthquakes: the two point correlation function. Geophys JR Astr Soc 62:303–320

Kanamori H (1977) The energy release in Great Earthquakes. J Geophy Res 82:2981–2987

Kanamori H (1983) Magnitude scale and quantification of earthquakes. Tectonophys 93:185–199

Mandelbrot BB (1983) The fractal geometry of nature. Freeman, New York

Mogi K (1962) Magnitude-frequency relationship for elastic shocks accompanying the fractures of various materials and some related problems in earthquakes. Bull Earthq Res Inst Univ Tokyo 40:831–883

Nandy DR (2001) Geodynamics of north eastern India and the adjoining region, 1st edn. ACB publications, Kolkata

Narenberg MAA, Essex C (1990) Correlation dimension and systematic geometric effects. Phys Rev A 42:7065–7074

Nuannin P, Kulhanek O, Persson L (2005) Spatial and temporal b value anomalies preceding the devastating off coast of NW Sumatra earthquake of December 26, 2004. Geophys Res Lett 32:L11307 DOI 10.1029/2005GL022679

Oncel AO, Wilson TH (2002) Space-time correlations of seismotectonic parameters: example from Japan and from Turkey preceding the Izmith earthquake. Bull Seism Soc Am 92:339–349

Oncel AO, Wyss M (2000) The major asperities of the 1999 M 7.4 Izmit earthquake, defined by the microseismicity of the two decades before it. Geophys J Int 143:501–506

Richter CF (1935) An instrumental earthquake magnitude scale. Bull Seis Soc Am 25:1–31

Ristau J, Rogers GC, Cassidy JF (2005) Moment magnitude–local magnitude calibration for earthquakes in western canada. Bull Seism Soc Am 95:1994–2000

Rong Y (2002) Evaluation of Earthquake Potential in China, PhD. Dissertation, Geophysics and Space Physics, University of California, Los Angeles

Schorlemmer D, Neri G, Wiemer S, Mostaccio A (2003) Stability and significance tests for *b* value anomalies: example from the Tyrrhenian Sea. Geophys Res Lett 30:1835 DOI 10.1029/2003GL017335

Scholemmer D, Wiemer S, Wyss M (2005) Variations in earthquake-size distribution across different stress regimes. Nature 437:539–542

Scholz CH (1968) The frequency-magnitude relation of microfracturing in rock and its relation to earthquakes. Bull Seism Soc Am 58:399–415

Scordilis EM (2006) Empirical global relations converting M_S and m_b to moment magnitude. J Seis 10:225–236

Stromeyer D, Grünthal G, Wahlström R (2004) Chi-square regression for seismic strength parameter relations, and their uncertainties, with applications to an Mw based earthquake catalogue for central, northern and northwestern Europe. J Seis 8:143–153

Suyehiro S, Asada T, Ohtake M (1964) Foreshocks and aftershocks accompanying a perceptible earthquake in central Japan: on the peculiar nature of foreshocks. Pap Meteorol Geophys 19:427–435

Thenhaus PC, Campbell W (2003) Seismic hazard analysis. In: Chen WF, Scawthorn C (eds) Earthquake engineering handbook. CRC Press, Boca Raton, pp 1–43

Turcotte DL (1986) A fractal model for crustal deformation. Tectonophysics 132:261–269

Utsu T (1965) A method for determining the value of b in the formula log N=a-bM showing the magnitude–frequency relation for the earthquakes. Geophys Bull Hokkaido Univ 13:99–103

Utsu T (1999) Representation and analysis of the earthquake size distribution: a historical review and some new approaches. Pageoph 155:509–535

Wesnouski SG, Scholz CH, Shimazaki K, Matsuda T (1983) Earthquake frequency distribution and the mechanics of faulting. J Geophys Res 88:9331–9340

Wiemer S, Wyss M (2000) Minimum magnitude of complete reporting in earthquake catalogs: examples from Alaska, the Western United States, and Japan. Bull Seism Soc Am 90:859–869

Willemann RJ, Storchak DA (2001) Data collection at the international seismological centre. Seis Res Lett 72:440–453

Woo G (1996) Kernel estimation methods for seismic hazard area source modeling. Bull Seism Soc Am 86:353–362

Wyss M, Sammis CG, Nadeau RM, Wiemer S (2004) Fractal dimension and *b* value on creeping and locked patches of the San Andreas Fault near Parkfield, California. Bull Seism Soc Am 94:410–421